# Experimental and Analytical Investigation of the Distortion of Turbulence Interacting with a Porous Airfoil

Zamponi, R.; Schram, C; Moreau, S.; Ragni, D.

**DOI**
10.2514/6.2021-2289

**Publication date**
2021

**Document Version**
Final published version

**Published in**
AIAA AVIATION 2021 FORUM

AIAA AVIATION Forum
August 2-6, 2021, VIRTUAL EVENT
AIAA AVIATION 2021 FORUM

10.2514/6.2021-2289



# Experimental and Analytical Investigation of the Distortion of Turbulence Interacting with a Porous Airfoil*

R. Zamponi† and C. Schram‡
*von Karman Institute for Fluid Dynamics, Sint-Genesius-Rode 1640, Belgium*

S. Moreau§
*Université de Sherbrooke, Sherbrooke J1K 2R1, Québec*

D. Ragni¶
*Delft University of Technology, Delft 2629 HS, the Netherlands*

**A possible strategy for the reduction of the aeroacoustic noise generated by turbulence interacting with a wing profile, also referred to as leading-edge noise, is represented by the implementation of a porous medium in the structure of the airfoil. However, the physical mechanisms involved in this noise mitigation technique remain unclear. The present work aims at elucidating these phenomena and particularly how the porosity affects the incoming turbulence characteristics in the immediate vicinity of the surface. A porous NACA-0024 profile integrated with melamine foam has been compared with a solid baseline, both airfoils being in turn subjected to the turbulence shed by an upstream cylindrical rod. The mean wall-pressure distribution along the airfoils shows that the implementation of the porous material mostly preserves the integrity of the NACA-0024 profile's shape. Results of hot-wire anemometry indicate that the porous design proposed in this study allows for damping of the velocity fluctuations and has a limited influence on the upstream mean flow field. Specifically, the upwash component of the root-mean-square of the velocity fluctuations turns out to be significantly attenuated in the porous case in contrast to the solid one. Furthermore, the comparison between the power spectral densities of the incident turbulent velocities demonstrates that the porosity has an effect mainly on the low-frequency range of the turbulent velocity power spectrum. This evidence is in line with the results of the acoustic beamforming measurements, which exhibit a noise abatement in an analogous frequency range. On the basis of these observations, an interpretation of the phenomena occurring in the turbulence-interaction noise reduction due to a porous treatment of the airfoil is finally given with reference to the theoretical inputs of the rapid distortion theory.**



## I. Nomenclature

| | | |
|---|---|---|
| $c$ | = | airfoil chord |
| $C_p$ | = | pressure coefficient |
| CSM | = | cross-spectral matrix |
| $d$ | = | cylindrical rod diameter |
| GIBF | = | generalized inverse beamforming |
| JCAL | = | Johnson-Champoux-Allard-Lafarge (model) |
| $k$ | = | static viscous permeability |
| $k'$ | = | static thermal permeability |
| $l$ | = | rectangular nozzle width |

*Parts of this paper are included in [1, 2].

†Postdoctoral researcher, Environmental and Applied Fluid Dynamics Department, riccardo.zamponi@vki.ac.be.

‡Ordinary Professor, Environmental and Applied Fluid Dynamics Department & Aeronautics and Aerospace Department, christophe.schram@vki.ac.be, AIAA member

§Ordinary Professor, Département de Génie Mécanique, stephane.moreau@usherbrooke.ca, AIAA member

¶Associate Professor, Aerodynamics, Wind Energy, Flight Performance & Propulsion Department, Faculty of Aerospace Engineering, d.ragni@tudelft.nl, AIAA member

$L_x$ = streamwise turbulence length scale
$p_\infty$ = static pressure in free-stream
$p_{\text{ref}}$ = reference sound pressure
$p_{0,\text{s}}$ = stagnation pressure of the solid airfoil
PSD = power spectral density
$r_{LE}$ = leading-edge radius
RDT = rapid distortion theory
$Re_d$ = Reynolds number based on the array diameter
$s$ = airfoil span
$TKE$ = turbulent kinetic energy
$t$ = airfoil maximum thickness
$\bar{U}$ = hot-wire mean velocity
$U'$ = hot-wire r.m.s of the velocity fluctuations
$U_\infty$ = free-stream velocity
$\alpha_\infty$ = tortuosity
$\Lambda$ = viscous characteristic length
$\Lambda'$ = thermal characteristic length
$\mu$ = dynamic viscosity of air
$\sigma$ = static air flow resistivity
$\Phi$ = one-dimensional turbulence spectrum of incident velocity
$\phi$ = porosity
$\xi$ = non-dimensionalized streamwise coordinate



## II. Introduction

The interaction between an airfoil and incident turbulence is an important source of aerodynamic noise in numerous applications that have a high societal impact, such as turbo engines, cooling systems for automotive and construction industries, or high-lift devices on aircraft wings. In these examples, the turbulence is generally produced by elements that are installed upstream of the airfoil and generate inflow distortions.

The turbulent eddies interacting with the leading edge are subjected to a rapid deformation that scatters part of their kinetic energy into sound [3]. A fundamental study on the noise emitted by this mechanism was performed by Amiet [4], who proposed a theory to predict the far-field acoustic power spectrum generated by an airfoil immersed in a turbulent flow. In this case, the spanwise correlation length and the integral length scale of the upwash turbulent velocity fluctuations constitute the key parameters for the prediction of the noise generated by the interaction with the incoming turbulence. Experimentally, the leading-edge noise generation process has been addressed by several authors. Paterson and Amiet [5] measured the emitted far-field noise and the unsteady surface pressure field of a NACA-0012 profile that was installed downstream of a turbulence grid and concluded that the prediction of incident turbulence-interaction noise can be carried out if the inflow properties are sufficiently documented. Olsen and Wagner [6] analyzed the broadband noise generated by the impingement of turbulence on airfoils characterized by different shapes and observed that an increasing thickness corresponded to a reduced turbulence-interaction noise. Similar conclusions were drawn by Oerlemans and Migliore [7], who performed wind tunnel tests for six different airfoils at several angles of attack in a grid-generated turbulent flow. Moreau et al. [8] investigated the effect of the angle of attack and the airfoil shape by studying the noise emitted by three different mock-ups (a flat plate, a thin controlled-diffusion (CD) airfoil, and a thick NACA-0012 profile) interacting with a turbulent flow in a grid-airfoil configuration. The results of the experiments confirmed the previously mentioned thickness effect, whereas the impact of the angle of attack and the camber was found to be limited. Devenport et al. [9] also confirmed the influence of the effects of these parameters by testing three airfoils in a wind tunnel that was equipped with a turbulence grid.

The effective distortion of the turbulent vortical structures at the leading edge must be taken into account in order to obtain an accurate prediction of the leading-edge noise when the airfoil exceeds a minimum thickness [8, 10, 11]. In this regard, a useful analytical tool that can be considered for estimating the turbulence distortion around an airfoil with a significant thickness is the rapid distortion theory (RDT), formulated by Hunt [12]. This theory assumes a particular distortion to occur rapidly enough to have a negligible contribution from the turbulence to the relative motion of the fluid particles when these are convected through the non-uniform mean flow region. In addition, the turbulent velocity fluctuations are supposed to be small compared with the free-stream velocity. Recently, experimental evidence of the

turbulence properties alteration that is predicted by the RDT for the case of a relatively thick airfoil was provided by Santana et al. [11].

Since acting on the turbulence intensity of the incident flow is typically unfeasible, one possible leading-edge noise mitigation strategy is to make the airfoil less affected by local disturbances. The usage of absorbing materials, e.g. porous media, as part of the airfoil structure has the potential of achieving such a goal, as firstly demonstrated by Lee [13], who numerically investigated the effect that a porous leading-edge insert of a helicopter blade had on the turbulence-interaction noise. He observed that a far-field noise reduction of up to 30 % was possible due to the suppression of the pressure fluctuations at the blade surface.

Geyer et al. [14, 15] manufactured numerous porous airfoils made of different materials and tested them with various grid-generated turbulent flows by means of microphone array techniques. They focused their attention on the influence of the parameters characterizing the porous media, observing how the noise-reduction performance was strongly related to the material properties. Particularly, they found that lower values of static air-flow resistivity could lead to more significant noise reduction but also to noise regeneration at high frequencies, most likely associated with the increased roughness due to the interaction of the airfoil boundary layer with the open pores of the material. Subsequently, the leading-edge noise produced by the same porous airfoils was investigated by Sarradj and Geyer [16] through symbolic regression tools. They observed a dependency of the noise on the square of the turbulence intensity and from the fifth to the sixth power of the flow velocity. The ratio of the integral length scale of the incoming turbulent flow to the characteristic length of the porous structure, linked to the static air-flow resistivity, was found to have a significant influence on the acoustic frequency spectrum.

When porosity covers the full chordwise extent of the airfoil, a noticeable deterioration of the aerodynamic performance is expected, resulting in a decrease of the lift force and an increase of the drag force, especially at high angles of attack [14, 17, 18]. The former effect is related to the communication between pressure and suction side of the wing profile through the pores of the material, whereas the latter effect is linked to the augmented surface roughness. Several researchers have already proposed technological solutions for the implementation of porous materials in the design of a wing profile with the aim of preserving its aerodynamic performance. Among them, Roger et al. [3] and Roger and Moreau [19] filled a NACA-0012 profile with steel wool to study the leading-edge noise reduction from a grid-airfoil and cylinder-airfoil interaction. They found that an attenuation ranging from 2.5 dB to 6 dB was achievable only for Strouhal numbers that were dependent on the characteristic length of the porous medium. A similar approach for the inclusion of porous materials in the structure of a thick airfoil has been proposed by Bampanis and Roger [20], who designed a rigid exoskeleton coated with a metallic wire mesh where melamine foam or metal wool could be fitted in. Likewise, a solid center plane was included to avoid cross-flow between pressure and suction side in order to maintain the aerodynamic performance of the wing profile. Broadband-noise mitigation varying from 4 dB to 6 dB was observed in this case.

Additional research on the application of a porous treatment of the airfoil was performed by Geyer et al. [21], who experimentally and numerically tested the effectiveness of perforated leading-edge inserts for the attenuation of grid-generated turbulence-interaction noise. Noticeable mitigation of up to 8 dB was achieved for frequencies ranging from 1 kHz to 4 kHz. Similar to previous investigations, noise regeneration occurring at high frequencies for perforated leading-edge inserts with large pores was found due to the increased surface roughness. A different design for a flow permeable insert has been investigated by Avallone et al. [22] and Sinnige et al. [23] with the aim of suppressing the noise produced by the interaction of a pylon with a propeller slipstream. Attenuation of the tonal components of the emitted far-field noise was measured in this case. Paruchuri et al. [24] studied the turbulence-interaction noise reduction obtained by flat plates characterized by different extents of porous inserts. Notably, they observed that the use of a single row of holes situated downstream of the leading edge allows for a significant low-frequency attenuation without increasing the noise radiations at higher frequencies.

All these studies demonstrated the potential of a porous treatment of the airfoil as a turbulence-interaction noise reduction technique. However, no definitive explanation about the physical mechanisms involved in noise mitigation has been found yet. One possible mechanism is linked to the dissipation of the acoustic energy by the viscous and thermal losses occurring during the oscillatory fluid motion in the pores of the material [25]. A second one is related to the hydrodynamic absorption of the turbulent eddies due to the interaction with a penetrable surface. As a consequence of this, the distortion experienced by the turbulence in the immediate vicinity of the airfoil may be affected by the porous treatment. The present research has the purpose of exploring the latter mechanism and builds upon the questions that have arisen in a previous piece of work where the noise-mitigation performance of a porous wing profile was assessed by comparing with a solid baseline [26]. An airfoil design in which melamine foam was implemented as part of the structure of a NACA-0024 profile has been proposed by the authors in that instance. The characterization of the

boundary layers around the two airfoil configurations showed the significant influence of porosity on the flow field and the acoustic far-field measurements demonstrated the effectiveness of the treatment. In addition, large-eddy simulations (LES) for the same experimental setup have been performed by Satcunanathan et al. [27] to predict the noise attenuation. Nonetheless, in both studies, no analysis of the turbulence distortion was carried out and no conclusions could be drawn on the noise reduction mechanisms.

The above-mentioned issues have been addressed in this paper, which expands on the results previously obtained [26, 27] and focuses on the analysis of the effects of porosity on the turbulence distortion. Further experiments have been carried out to better investigate this aspect, whose interpretation constitutes the true added value of the present research. This measurement campaign has been conducted in the JAFAR facility of the von Karman Institute for Fluid Dynamics (VKI). The solid and porous cases have been compared considering a zero-lift angle of attack and a jet outlet flow speed of $30\,\mathrm{m\,s^{-1}}$. The incident turbulence has been generated by placing a cylindrical rod upstream of the airfoil. In this arrangement, firstly proposed by Jacob et al. [28] as an aeroacoustic benchmark problem, the airfoil undergoes a broadband perturbation dominated by a shedding frequency, similar to what is commonly observed behind bluff bodies such as landing gears. The experimental investigation presented in the paper involves the measurement of the far-field noise with a phased-microphone array, the study of the mean wall-pressure distribution on the surface of the airfoils, and the characterization of the mean and unsteady flow field in the stagnation region using a single-sensor hot-wire probe. Subsequently, the power spectra of the velocity fluctuations measured by the hot-wire are computed in order to analyze whether they can be linked to the acoustic power spectra. Finally, the experimental results will be compared with the analytical prediction given by the RDT model recently proposed by Zamponi et al. [29], who extended the theory in order to account for a porous body.

The paper is structured as follows: the measurement setup is presented in Section III. Section IV describes the experimental results, highlighting the turbulence distortion effects in the stagnation region, whereas in Section V the results are discussed considering the analytical inputs of the RDT. Finally, conclusions are drawn in Section VI.



## III. Materials and methods

### A. Rod-airfoil configuration

Figure 1 shows a sketch of the rod-airfoil configuration installed in the JAFAR facility of VKI. A circular-to-rectangular contraction designed by de Santana [30] adapts the circular geometry of the upstream duct to the rectangular geometry of the exhaust nozzle. The area ratio is 2.35 to 1 and the nozzle exit has a span of $s = 0.200\,\mathrm{m}$ and a width of $l = 0.150\,\mathrm{m}$. Two side plates guide the flow and support the $d = 0.020\,\mathrm{m}$ diameter cylindrical rod and the NACA-0024 profile, separated from each other by a distance of $0.174\,\mathrm{m}$ ($x/d = 8.20$). The airfoil chord is $c = 0.157\,\mathrm{m}$ ($c/d = 7.85$) and the maximum thickness is approximately $t = 0.038\,\mathrm{m}$ ($t/d = 1.90$). This value has been designed in order to have the same radius for the airfoil leading edge and the rod.

Given the relatively low aspect ratio $s/c = 1.27$ of the airfoil, some precautions are taken to minimize the risk of contamination of the acoustic field by corner effects. Indeed, the junctions between the airfoil and side plates are filled with a rounded fillet of clay with a radius approximately equal to $0.003\,\mathrm{m}$ that has the primary function to avoid gap noise [31]. Moreover, the thickness of the incoming boundary layer over the side plates is found to be less than $0.002\,\mathrm{m}$ and is characterized by a turbulence intensity well below that of the incoming turbulence in the main stream.

The following reference system, indicated by the red arrows in Fig. 1, has been adopted for the presentation of the results: the $x$-axis is aligned with the flow direction, the $z$-axis is aligned with the spanwise direction of the airfoil, and the $y$-axis is oriented in the normal direction in order to form a right-handed coordinate system. The origin is set at the midspan and at the leading edge of the airfoil mock-up.

### B. Design of the airfoils

The same manufacturing technique has been used to design the solid and the porous versions of the airfoil. For both of them, a hard plastic exoskeleton with a thickness of $0.002\,\mathrm{m}$ preserves the structural integrity of the model. This is made of two components, one per each side of the airfoil surface, which have been glued together at the leading edge and the trailing edge. The porous airfoil exoskeleton features hexagonal openings throughout its surface, with a side-to-side length of $0.004\,\mathrm{m}$ and an equivalent open area ratio of 80 % to allow for the penetration of the air flow into the inner region. Figure2 illustrates a schematic of this component. The volume of the airfoil has been filled with melamine foam. A hard plastic impenetrable center-plane avoids the cross-flow between the two sides of the wing profile. However, its

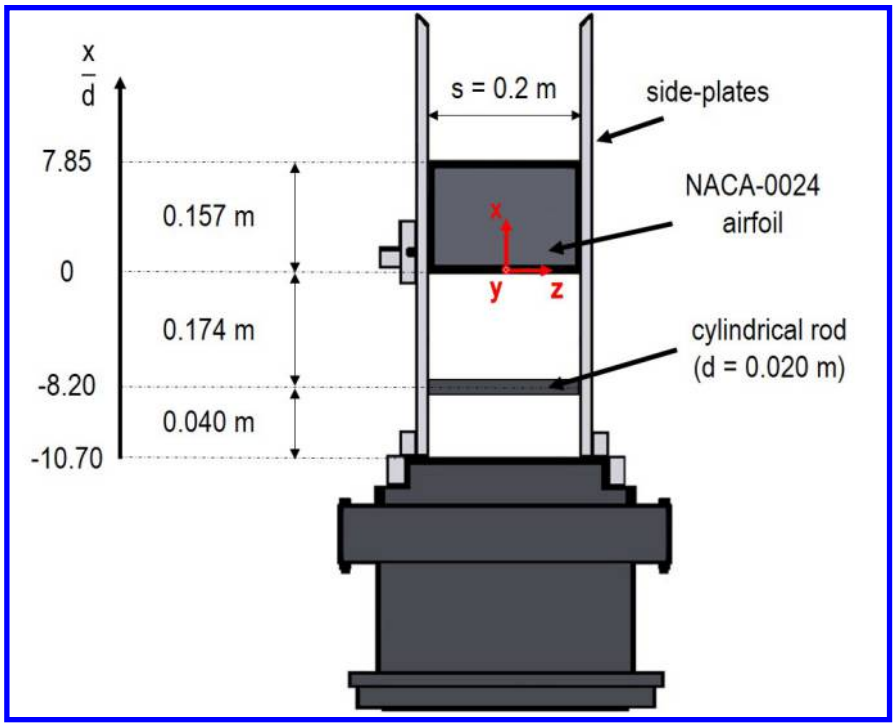


**Fig. 1 Sketch of the rod-airfoil configuration installed in the JAFAR facility of VKI. The red arrows denote the coordinate axes of the reference system.**

extent does not cover the first 6.4 % of the chord (one leading-edge radius) to allow for the penetration of the air flow at the stagnation point. Moreover, both airfoils have been coated with the same metallic woven wire mesh, which protects the materials and guarantees an adequate quality surface roughness. This is characterized by an aperture of 0.198 mm, a wire diameter of 0.056 mm, and an open area ratio of 60.8 %. Figure 3a provides a sketch of the different parts of the porous airfoil, whereas a picture of the two manufactured prototypes is shown in Figs. 3b and 3c.

Finally, the solid and the porous airfoils have been equipped with 35 static pressure sensors distributed along both sides of the airfoils, at corresponding streamwise locations (Fig. 3c). The transducers have been placed at the corners of the hexagonal openings in the midspan of the exoskeleton, thereby minimizing the alterations of the local open area ratio, as shown in Fig. 2. The $x$-coordinates of the sensors range from 1 % to almost 80 % of the chord. Furthermore, an additional measurement position has been designed at the airfoil leading edge in order to acquire the stagnation pressure. The ports have then been connected to an in-house acquisition system for the evaluation of the mean wall-pressure distributions and the data have been acquired at a sampling frequency of 500 Hz, with an acquisition time of 15 s.

### C. Characterization of the porous medium

According to the Johnson-Champoux-Allard-Lafarge (JCAL) model [32–34], the six parameters that are necessary to fully characterize the porous material are the static air-flow resistivity, $\sigma$, the porosity, $\phi$, the tortuosity, $\alpha_\infty$, the viscous characteristic length, $\Lambda$, the thermal characteristic length, $\Lambda'$, and the static thermal permeability, $k'$. Besides these, another property used to define a porous medium is the static viscous permeability, $k$, which is directly linked to $\sigma$ by the relationship $k = \mu/\sigma$, $\mu$ being the dynamic viscosity of air.

The characterization of the melamine foam parameters has been carried out in collaboration with the Laboratoire d'Acoustique de l'Université du Maine (LAUM). An inverse method based on the measurement of the scattering matrix by means of a 4-microphone impedance tube has been adopted [35]. The results are listed in Table 1. Furthermore, additional measurements have been performed at Centre de Transfert de Technologie du Mans (CTTM) using samples of the exoskeleton and the wire mesh. The static air-flow resistivity of the two layers has been found to be negligible compared with that of the melamine foam. The measured parameters have been used by Satcunathan et al. [36] for calibrating and validating a direct hybrid LES/CAA method.

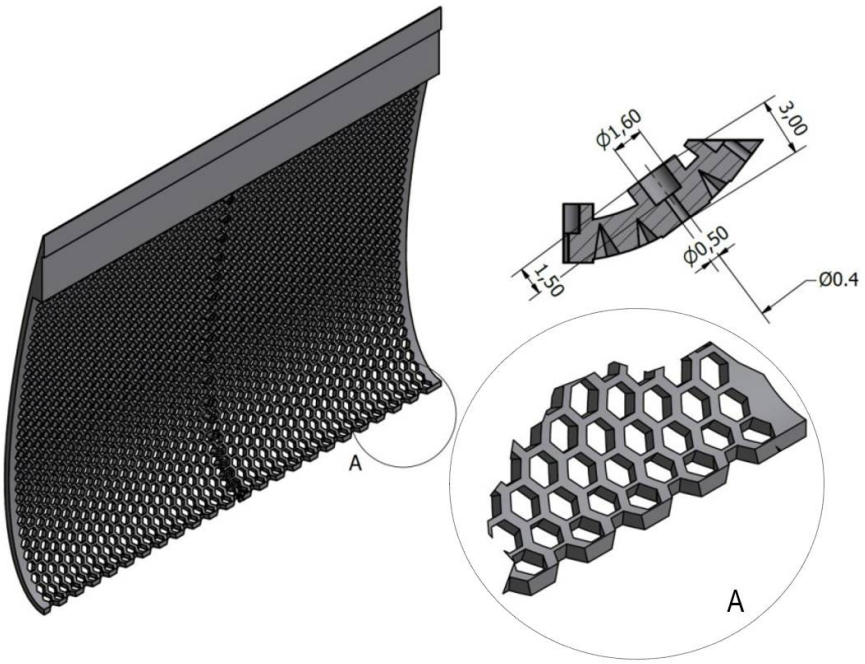


**Fig. 2 Structure of the permeable exoskeleton exhibiting the hexagonal openings and the static pressure port.**

**Table 1 JCAL model parameters characterizing the melamine foam of the porous airfoil.**

| $\sigma$ [Pa s m$^{-2}$] | $\phi$ [-] | $\alpha_\infty$ [-] | $\Lambda$ [m] | $\Lambda'$ [m] | $k'$ [m$^2$] |
|---|---|---|---|---|---|
| $8.683 \times 10^3$ | $9.86 \times 10^{-1}$ | 1.02 | $1.344 \times 10^{-4}$ | $1.942 \times 10^{-4}$ | $2.305 \times 10^{-9}$ |

### D. Nozzle flow qualification

The experiments have been carried out at a free-stream flow velocity of $U_\infty = 30\,\mathrm{m\,s^{-1}}$ that corresponds to a Reynolds number based on the rod diameter of $Re_d = 4.1 \times 10^4$. The airfoil is set at 0° angle of attack, which has been verified by the mean wall-pressure distribution.

Profiles of the mean streamwise velocity, $\bar{U}$, and of the root-mean-square (r.m.s.) of the streamwise velocity fluctuations, $U'$, have been obtained at the nozzle exit with a single hot-wire L-shaped probe. This has been connected to an in-house anemometer and installed in a carriage system, depicted in Fig. 4, that enables the automatic movement of the sensor within the $yz$ plane. The static calibration of the hot-wire has been performed in-situ on a daily basis, using a Prandtl tube to measure the reference velocity. All the measurements have been corrected in order to take into account the temperature variations during the tests by following the method proposed by Bruun [37]. The sampling frequency has been set to 51.2 kHz, which has led to an anti-aliasing filter set to 25.6 kHz, and the data have been acquired for a duration of 5 s to keep the maximum relative uncertainty below 0.4 % for the mean velocity in the potential core of the jet.

Figures 5a and 5b present the dimensionless mean velocity, $\bar{U}/U_\infty$, and the turbulence intensity, $U'/U_\infty$, along the $y$-axis at $z = 0$, respectively. The probe has been placed 0.001 m downstream of the nozzle exit in the streamwise direction, corresponding to $x/d = -10.65$. The cylindrical rod has been removed to allow for the movement of the sensor. The mean velocity remains within 4 % of $U_\infty$ across the potential core of the jet, whereas an increase of up to 9 % of $U_\infty$ can be observed in proximity to the nozzle edges. The sharp transition in the velocity between the potential core and the no-flow region indicates a limited width for the shear layer, as would be expected at such a short distance from the nozzle exit. In Fig. 5b, the turbulence intensity is found to be about 0.4 % in the potential core of the jet. Finally, the peaks in turbulence intensity are located in the two shear layer regions and amount to almost 10 %, with an uncertainty below 1.4 %.

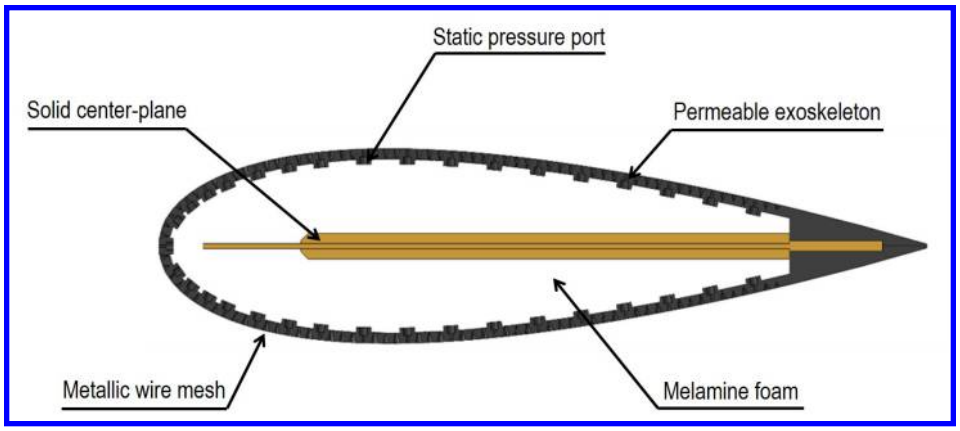


(a)

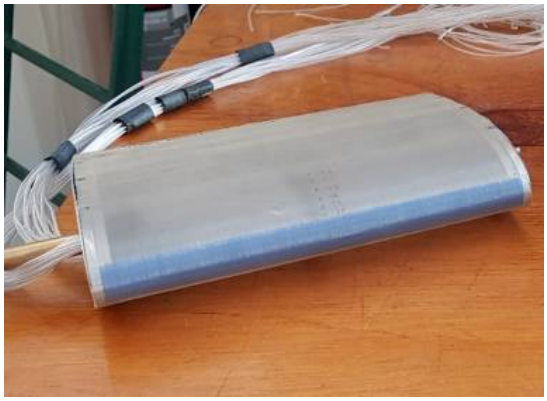

(b)

(c)

**Fig. 3 (a) Representation of the porous NACA-0024 profile featuring the solid center-plane, the hard-plastic exoskeleton, the metallic wire mesh, and the static pressure ports. (b)-(c) Pictures of the solid airfoil (on the left) and the porous airfoil (on the right) manufactured at VKI.**

### E. Flow field characterization

The investigation of the stagnation region surrounding the airfoil leading edge has been conducted using the same hot-wire anemometer employed for the nozzle flow qualification. In this case, the carriage system has been rotated in order to enable the movement of the sensor along the $x$-direction. The wire has been mounted on a straight probe oriented perpendicularly to the flow direction. The sampling frequency has been set to 51.2 kHz, whereas the acquisition time has been extended to 10 s in order to ensure statistical convergence in the computation of the velocity power spectral density (PSD) of the incident velocity fluctuations. The PSDs have been obtained with Welch periodogram method [38], with blocks of $2^{13}$ samples windowed using a Hanning weighting function that is characterized by a 50 % data overlap, thus providing a frequency resolution of 6.25 Hz. Furthermore, the temperature variations have been corrected by following the model proposed by Bruun [37].

Figure 6 illustrates the measurement positions of the single traverse acquired along the stagnation streamline. The $x$-coordinate is normalized by the leading-edge radius, $r_{LE}$. The traverse has been designed at $z = 20$ mm (10 % of the airfoil span) in order to avoid the influence of the static pressure port on the measurement points close to the wing profile's surface. 55 locations have been considered, with the probe moving in the streamwise direction from the upstream flow region towards the airfoil leading edge. The distance between consecutive measurement positions varies from 2.0 mm, to 1.0 mm, and finally to 0.5 mm as shown in Fig. 6. The minimum distance of the probe from the surface less than 0.5 mm has been evaluated using a dummy sensor having the same geometry as the hot-wire probe. In this way, it has been possible to optically determine the exact position at which the prongs of the sensor touch the surface of the airfoil at the leading edge without harming the actual probe.

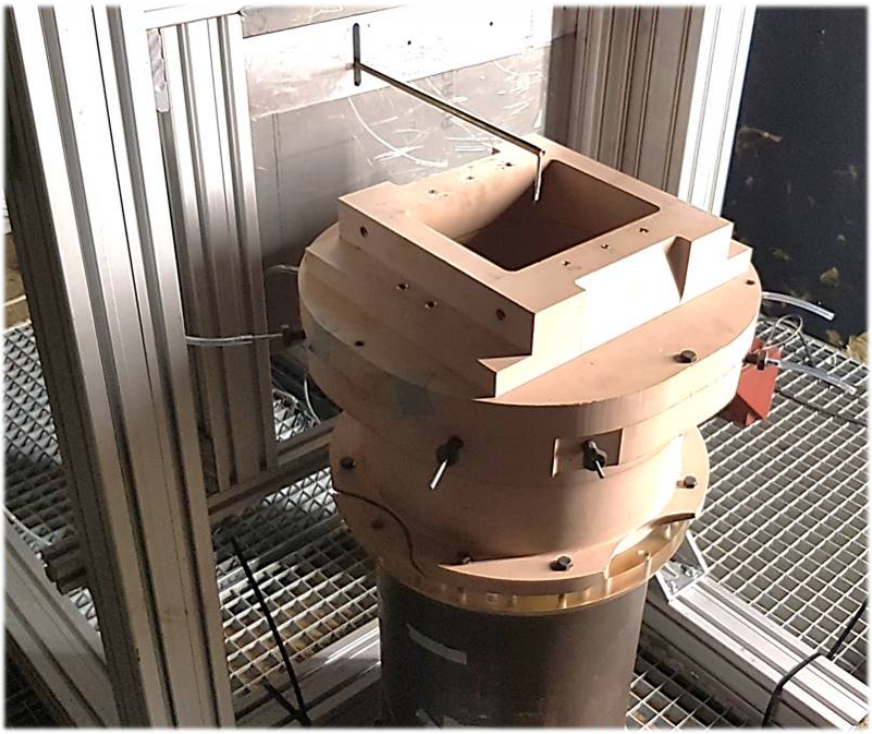

**Fig. 4 Carriage system installed in the JAFAR facility for the automatic movement of the hot-wire L-shaped probe within the $yz$ plane for the qualification of the facility.**

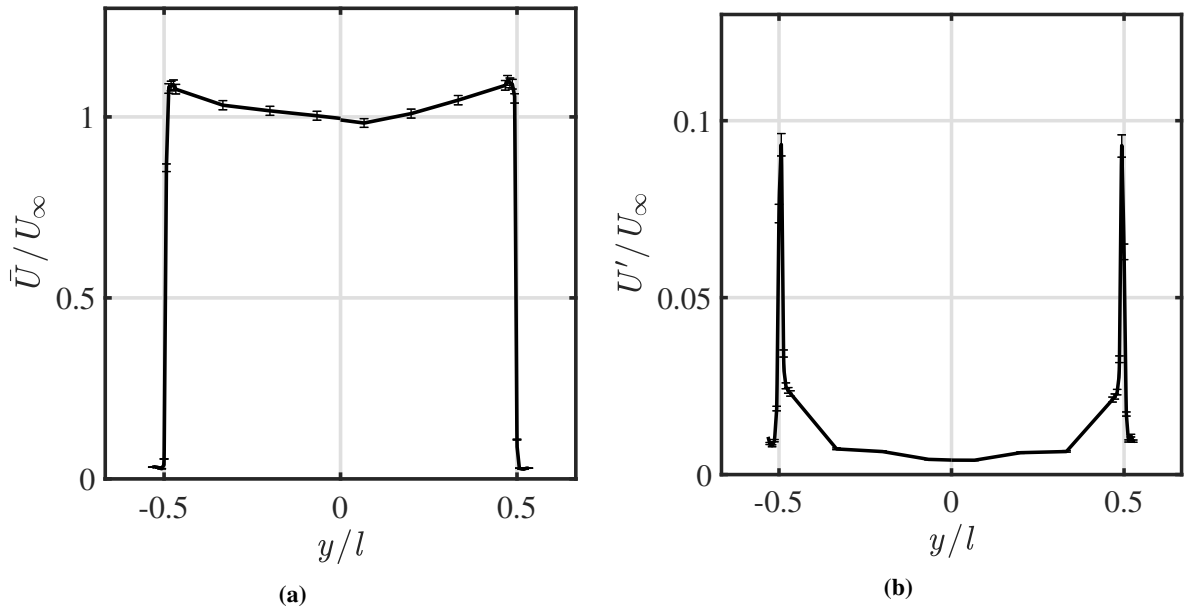


**Fig. 5 Mean-velocity (a) and turbulence-intensity (b) profiles at $x/d = -10.65$, corresponding to $x = -0.213$ m, at the airfoil midspan.**

### F. Acoustic beamforming setup

The noise reduction performance that is achieved with a porous treatment of the airfoil has been evaluated by means of acoustic beamforming. A seven arms Dougherty array [39] has been used for the measurements. This has been placed at 1.160 m from the airfoil, out of the flow, and its center has been approximately aligned with the midspan of the airfoil

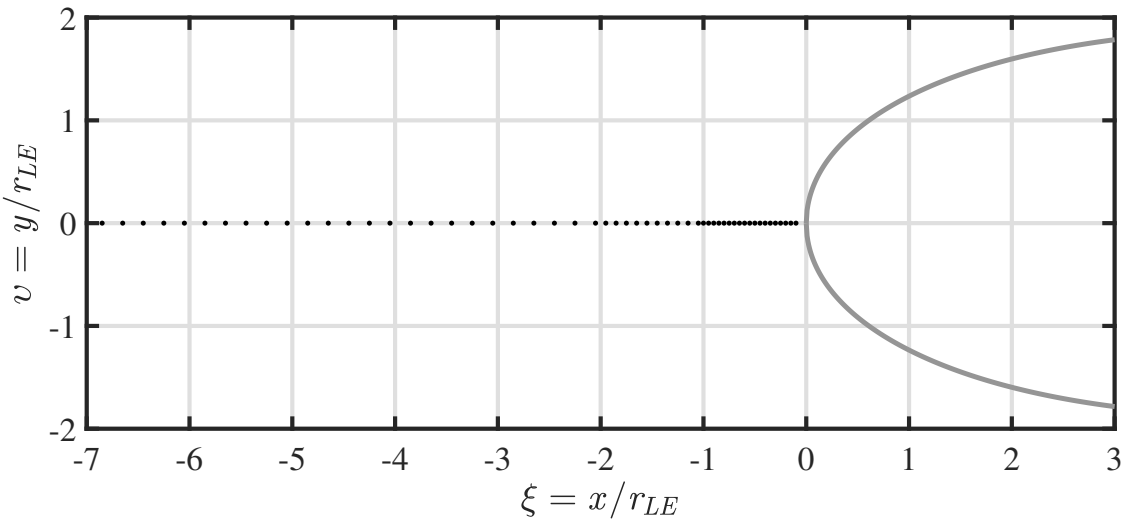


**Fig. 6 Traverse designed for the characterization of the stagnation streamline by means of hot-wire anemometry consisting of 55 points at $z = 0.1s$. The distance between the points is 2.0 mm, 1.0 mm and 0.5 mm for the first 50 mm ($5r_{LE}$), the following 10 mm ($1r_{LE}$), and the final 10 mm ($1r_{LE}$) of the traverse, respectively, whereas the minimum distance of the probe from the surface is 0.5 mm.**

leading edge. The array has an aperture of 1.5 m and is equipped with 64 capacitor-based Knowles electret microphones model FG-23329-P07 (frequency response: ±3 dB; frequency range: from 100 Hz to 10 kHz), calibrated in amplitude and in phase. Figure 7a depicts the projection of the central microphone positions on the scanning grid plane. The data have been acquired at a sampling frequency of 51.2 kHz for 60 s. The cross-spectral matrix of the measured signals has been computed by employing the Welch method [38], with blocks of $2^{13}$ samples windowed using a Hanning weighting function that is characterized by a 50 % data overlap, thus providing a frequency resolution of 6.25 Hz.

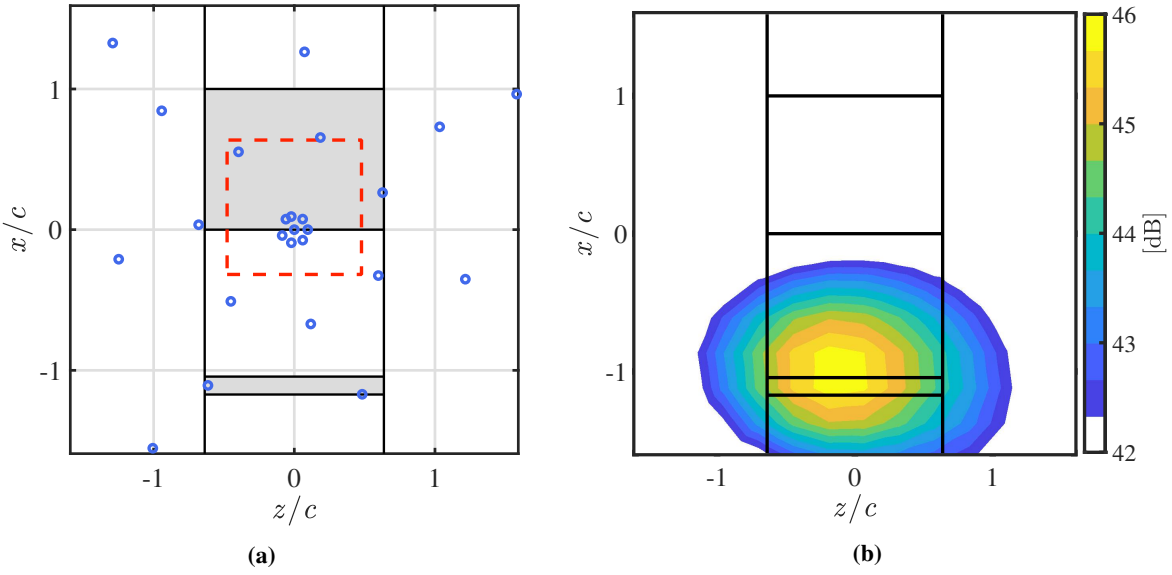


**Fig. 7 (a) Configuration of the GIBF sound map, with the black lines indicating side-plates, rod, and airfoil leading edge and trailing edge, the red dashed lines denoting the source integration area, and the blue dots illustrating the projection of the central microphones positions on the scanning grid plane. (b) GIBF sound map for the solid airfoil at $f_{1/3} = 250$ Hz computed with a reference pressure $p_{\mathrm{ref}} = 20\,\mu$Pa. No background noise removal has been applied.**

The acoustic data have been post-processed using a generalized inverse beamforming (GIBF) technique developed at VKI and validated with both numerical and experimental benchmark datasets [40–43]. Corrections to account for the convection of the flow and the refraction of the shear layer have been applied by following the method proposed by Sijtsma [44]. The use of an advanced beamforming algorithm turns out to be crucial to properly isolate the different noise source contributions coming from the open jet, the rod self-noise, and the noise sources generated at the juncture of the side-plates and the airfoil due to the scattering of the turbulent boundary layer forming along with the plates. Particularly, the rod noise has been found to be the dominant source for a major part of the sound frequency spectrum, making it difficult to measure the leading-edge noise produced by the airfoil with a single microphone. This is a consequence of the thickness effect of the NACA-0024 profile that decreases the efficiency of the noise generation mechanism, as mentioned in Section II.

Proper handling of the background noise is also required to ensure better evaluation of the sound maps. Hence, the advanced subtraction technique developed by Bahr and Horne [45] has been employed. In this case, the acquired background noise corresponds to a configuration where the airfoil has been removed. Indeed, the distance between the rod and the airfoil is such that the vortex shedding is not suppressed by the presence of the body and the vortex-shedding frequency remains unaltered, making it feasible to perform the subtraction. An example of a GIBF sound map where no background noise removal has been applied is reported in Fig. 7b. The map refers to the solid airfoil and has been computed at the one-third octave band center frequency $f_{1/3} = 250\,\text{Hz}$ and with a reference pressure of $p_{\text{ref}} = 20\,\mu\text{Pa}$.

Moreover, GIBF is based on the eigenvalue decomposition of the cross-spectral matrix of the microphone signals and each eigenvalue is linked to a coherent source distribution under the constraint of orthogonality [46]. This feature makes it possible to select a subset of eigenmodes to process, which corresponds only to the actual sources of interest, such as those generated by turbulence-interaction. A similar approach has been followed by Zamponi et al. [47] for characterizing the aeroacoustic noise sources of a counter-rotating open rotor by means of GIBF. In the present investigation, one eigenmode has been found to be dominant for each frequency after the background subtraction and, therefore, has been computed by the algorithm.

An extensive analysis of the acoustic beamforming sound maps has been already reported in Zamponi et al. [26]. In that instance, the investigation was limited to the one-third octave band center frequencies ranging from 1 kHz to 5 kHz and a significant noise increase was observed starting from 2 kHz. The origin of this phenomenon can be attributed to the presence of the exoskeleton that induces a cross-flow within its hexagonal pores and alters the surface roughness.

The focus of the present analysis is on the low-frequency range in order to investigate the noise reduction around the vortex shedding frequency. At low frequencies, the resolution of the beamforming sound maps is typically too low to exhibit a clear representation of the distributed noise sources along the leading edge due to the beamwidth characteristics of the microphone array. Nevertheless, the information on the source strength is preserved and it can be evaluated by integrating the sound maps after their decontamination from the background noise. The integration is then performed by summing the pressure values of each scanning grid point within a square region surrounding the airfoil leading edge.

A sketch of the experimental setup to yield the sound maps is illustrated in Fig. 7a. The scanning grid ranges between $-2 < z/c < 2$ and $-2 < x/c < 2$, with a spatial resolution of 0.01 m. The vertical black lines indicate the test section side walls, the cylindrical rod, the leading edge, and the trailing edge of the airfoil. The red dashed lines indicate the considered integration area, which is located within the potential core of the jet and has a dimension of $0.15\,\text{m} \times 0.15\,\text{m}$.



## IV. Results

In this section, the results of acoustic beamforming are first presented. Subsequently, the influence that the porous material has on the flow field around the solid and porous airfoil is analyzed through mean wall-pressure distribution measurements. Finally, the outcomes of the experimental and investigation of the flow field alterations within the stagnation region are discussed.

### A. Aeroacoustic Measurements

Figs. 8a and 8b show the GIBF sound maps for the solid and the porous airfoils, respectively, and refer to the one-third octave band center frequency $f_{1/3} = 250\,\text{Hz}$, which corresponds to the band that includes the vortex shedding frequency. The maps provide the one-third octave band sound pressure level $L_{\text{p(1/3)}}$ calculated with a reference pressure of $p_{\text{ref}} = 20\,\mu\text{Pa}$ and they are presented considering the same dynamic range of 12 dB. As already mentioned in Section III.F, the noise source region does not appear distributed at the leading edge but extends over most of the airfoil surface for both solid and porous cases. Nevertheless, the adopted dynamic range allows for visual estimation of the noise

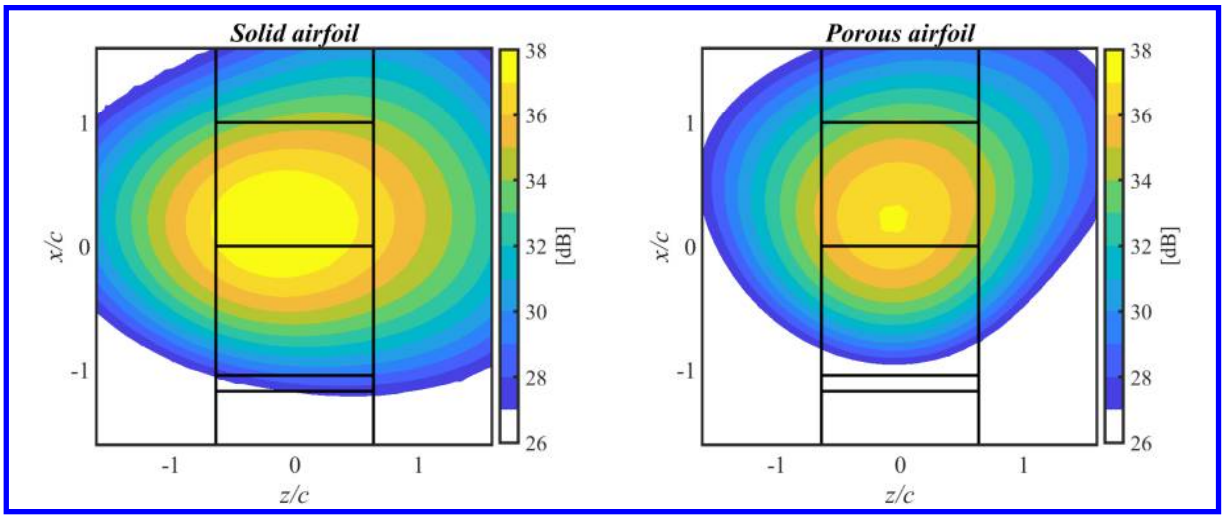


**Fig. 8 GIBF sound maps exhibiting the noise source distribution contours for the (a) solid and (b) porous airfoil at $f_{1/3} = 250$ Hz. The maps are plotted with the same 12 dB dynamic range for both cases and computed with a reference pressure of $p_{ref} = 20\,\mu$Pa. A background subtraction technique is applied to reduce the rod-noise contribution.**

reduction achieved at this frequency range due to the porous treatment.

Furthermore, inverse beamforming methods such as GIBF display the source distribution contours instead of the peak source intensity, differently from direct techniques [46]. Hence, the integration of the maps is required to assess the actual noise source strength. This explains the relatively low levels of the sound maps in Fig. 8.

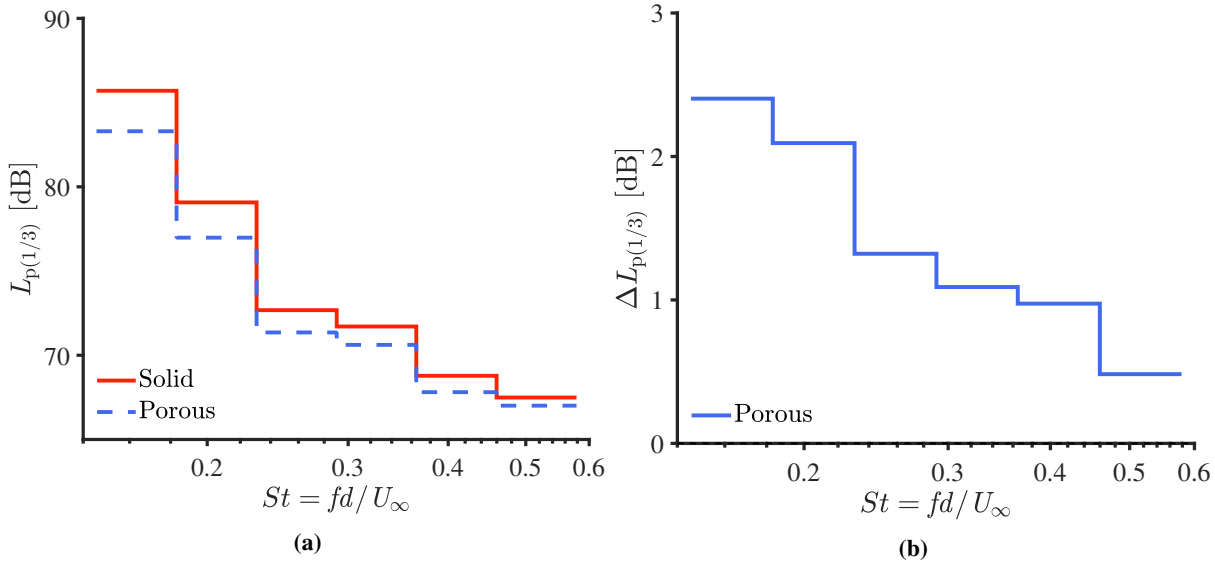


**Fig. 9 (a) GIBF integrated one-third octave band spectra referred to the one-third octave band center frequencies ranging from 250 Hz to 800 Hz for the solid airfoil (red solid line) and the porous airfoil (blue dash-dotted line) and computed with a reference pressure of $p_{ref} = 20\,\mu$Pa. (b) Relative noise reduction due to the porous treatment of the airfoil with respect to the solid case.**

The resulting sound maps for one-third octave band center frequencies ranging from 250 Hz to 800 Hz have been subsequently integrated with reference to the center of the array. The integrated spectra for both airfoils are presented in

Fig. 9a, whereas the relative one-third octave band sound pressure level $\Delta L_{p(1/3)}$ of the porous airfoil with respect to the solid one is shown in Fig. 9b for a better representation of the noise reduction. The greatest abatement occurs at lower frequencies, in correspondence with the band containing the tonal component at the shedding frequency, and amounts to about 2.5 dB. For higher $St$, the noise mitigation gradually decreases and solid and porous spectra start converging.

However, the noise reduction performance achieved in the present work appears to be low if compared to the results of the investigations discussed in Section II. This limited efficiency may be related to the presence of the exoskeleton that decreases the flow penetration into the melamine foam. Another possible explanation for the lower performance of the porous treatment is represented by the center-plane. Indeed, the acoustic waves generated on the airfoil surface can potentially penetrate the porous medium and interact with the solid walls of this component, similarly to the effect of the material junctions in the case of a porous leading-edge insert [48]. Further parametric studies will be performed in the near future to analyze the influence of the center-plane on the noise reduction.

### B. Static pressure distribution

The results of the mean wall-pressure distribution measurements are presented by defining the pressure coefficient $C_p$ as

$$C_p = \frac{p - p_\infty}{p_{0,s} - p_\infty}, \tag{1}$$

where $p$ is the measured mean wall-pressure and $p_\infty$ and $p_{0,s}$ are the static pressure in the free-stream and the stagnation pressure measured at the leading edge of the solid airfoil, respectively.

The $C_p$ distributions along the chord for the solid and porous airfoils are shown in Fig. 10. Each point of the curve has been calculated by averaging the mean wall pressure acquired on the two sides of the airfoil at the same chord position.

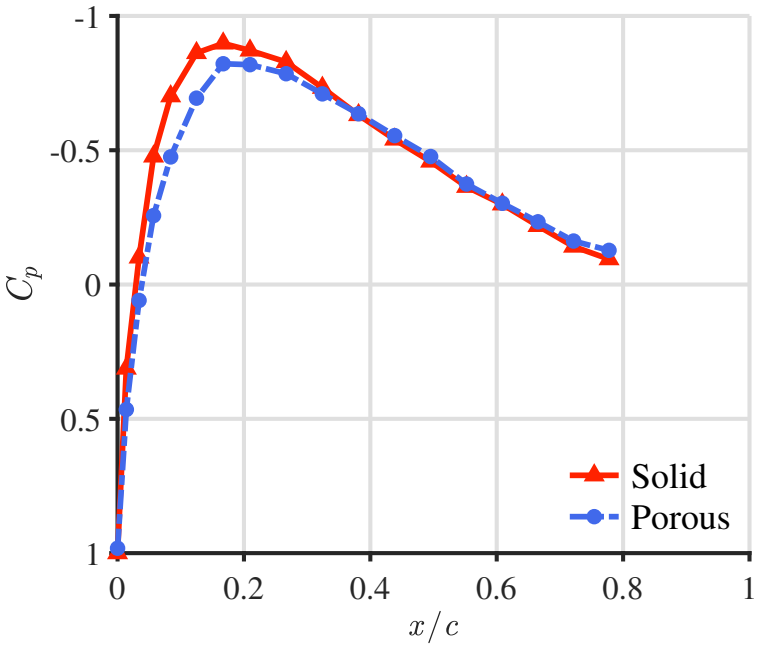


**Fig. 10 $C_p$ distribution along the airfoil chord measured for the solid (red solid line) and the porous (blue dash-dotted line) airfoil for $U_\infty = 30\,\mathrm{m\,s^{-1}}$ and for a $0°$ angle of attack.**

The alteration of the mean pressure field by the porous treatment appears to be mostly confined to the upstream 30 % of the airfoil, despite the fact that the melamine foam fills the porous airfoil up to 80 % of the chord. Nonetheless, the pressure recovery experienced by the solid NACA-0024 profile downstream of the maximum thickness is slightly higher than that in the porous case, with a deviation that increases as the trailing edge is approached. The maximum difference at $x/c = 0.8$ is approximately $|\Delta C_p| = 0.03$. The present trend agrees with the thicker boundary layer that has been observed in the aft part of the porous airfoil in previous works [26, 27]. Furthermore, the two configurations exhibit

almost the same pressure at the stagnation point, although this value does not correspond to the free-stream dynamic pressure since the airfoil is immersed in the wake of the rod.

The negative $C_p$ peak for the two airfoils occurs at 17 % of the chord and is almost preserved, being its absolute value reduced by 6.7 % in the porous case. Moreover, for the porous airfoil, this peak is reached in a more gradual way. The discrepancy can be explained by the partial penetration of the air flow through the pores of the melamine foam that tends to level out the pressure differences along the surface and reduces the flow displacement by the NACA-0024 profile. This would most likely degrade the lift of the airfoil if placed at some non-zero angle of attack, as reported in similar works [17, 49].

### C. Mean and fluctuating velocity field along the stagnation streamline

The hot-wire anemometry results indicate that the implementation of the porous material in the airfoil structure preserves the potential effect with regard to the upstream flow. Figure 11a illustrates the mean-velocity profile along the stagnation streamline for the solid and the porous airfoils. $\bar{U}$ is normalized by the free-stream velocity. As can be observed, the experimental data for the two cases follow the same trend up to the immediate vicinity of the leading edge. This conclusion is supported also by the relatively small deviation in the solid and porous $C_p$ distributions of Fig. 10.

The most striking effect of porosity is on the evolution of the turbulent velocity fluctuations in the immediate vicinity of the leading edge. The turbulence-intensity profile along the stagnation streamline for the solid and the porous airfoil is depicted in Fig. 11b. As can be seen from the plot, the experimental data present a similar trend up to about $0.5r_{LE}$ from the leading edge, with a constant value equal to 1 for $\xi < -2$ and a decrease in the region $-2 \leq \xi < -0.5$. Above this threshold, the solid and the porous cases diverge significantly, the former starts to increase and the latter keeps decreasing.

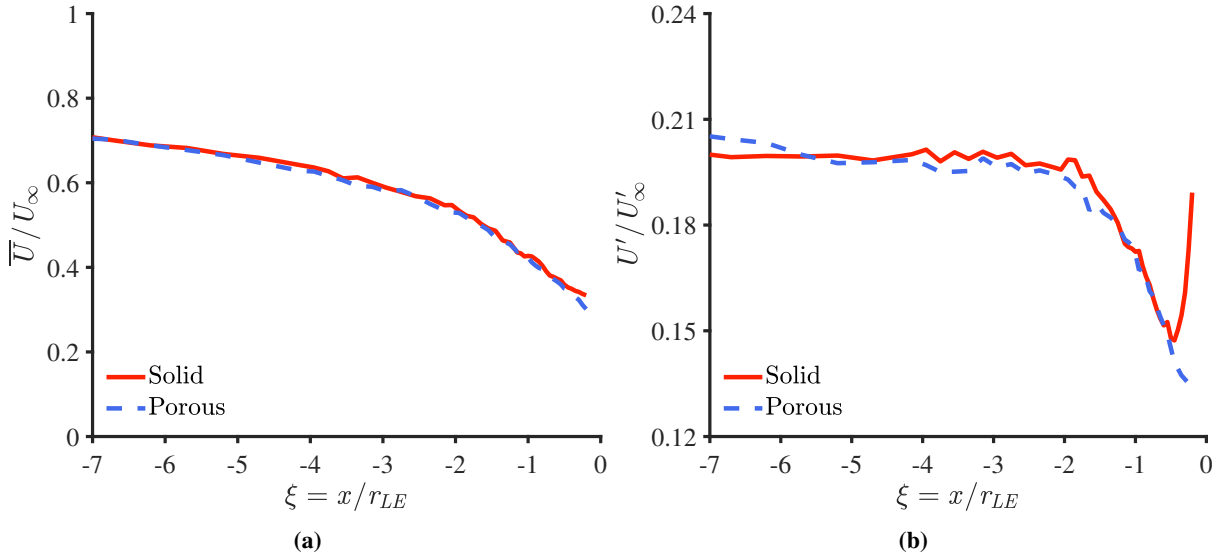


**Fig. 11 Mean-velocity profile (a) and turbulence-intensity profile (b) of the solid (in red) and porous (in blue) airfoil along the stagnation streamline for $U_\infty = 30\,\mathrm{m\,s^{-1}}$ and for a $0^\circ$ angle of attack.**

For small turbulence levels, a single normal hot-wire responds only to fluctuations in the direction of the mean velocity [50]. Therefore, in the region for $\xi < -2$, where the flow has a preferred direction along the $x$-axis, $U'$ is dominated by the streamwise velocity fluctuations, which are constant. When the stagnation region is being approached, these are attenuated accordingly with the decrease of mean velocity due to the potential effect of the airfoil. However, near the stagnation point, the mean flow field further reduces and the hot-wire detects also the velocity fluctuations in the $y$-direction. This assumption is verified by the trend observed for the solid case, where the contribution of the upwash component of the velocity fluctuations is visible. In this case, indeed, the no-penetration condition imposed by the rigid surface forces the streamwise velocity fluctuations to be zero, leading to a transfer of momentum to the upwash component. This is the origin of the strong increase of velocity fluctuations in Fig. 11b for the solid airfoil.

In view of the above, it is possible to relate the damping effect of the porosity on $U'$ to the attenuation of the upwash component of the velocity fluctuations. This outcome is in agreement with the analysis on the numerical

results conducted by Satcunanathan et al. [27], where a strong attenuation of the turbulent kinetic energy (TKE) in the stagnation region of the porous airfoil was reported. The present result constitutes a key point to understand the physical mechanism for which the porous treatment of the airfoil affects the turbulence distortion and will be discussed in Section V.

### D. Turbulent velocity power spectra

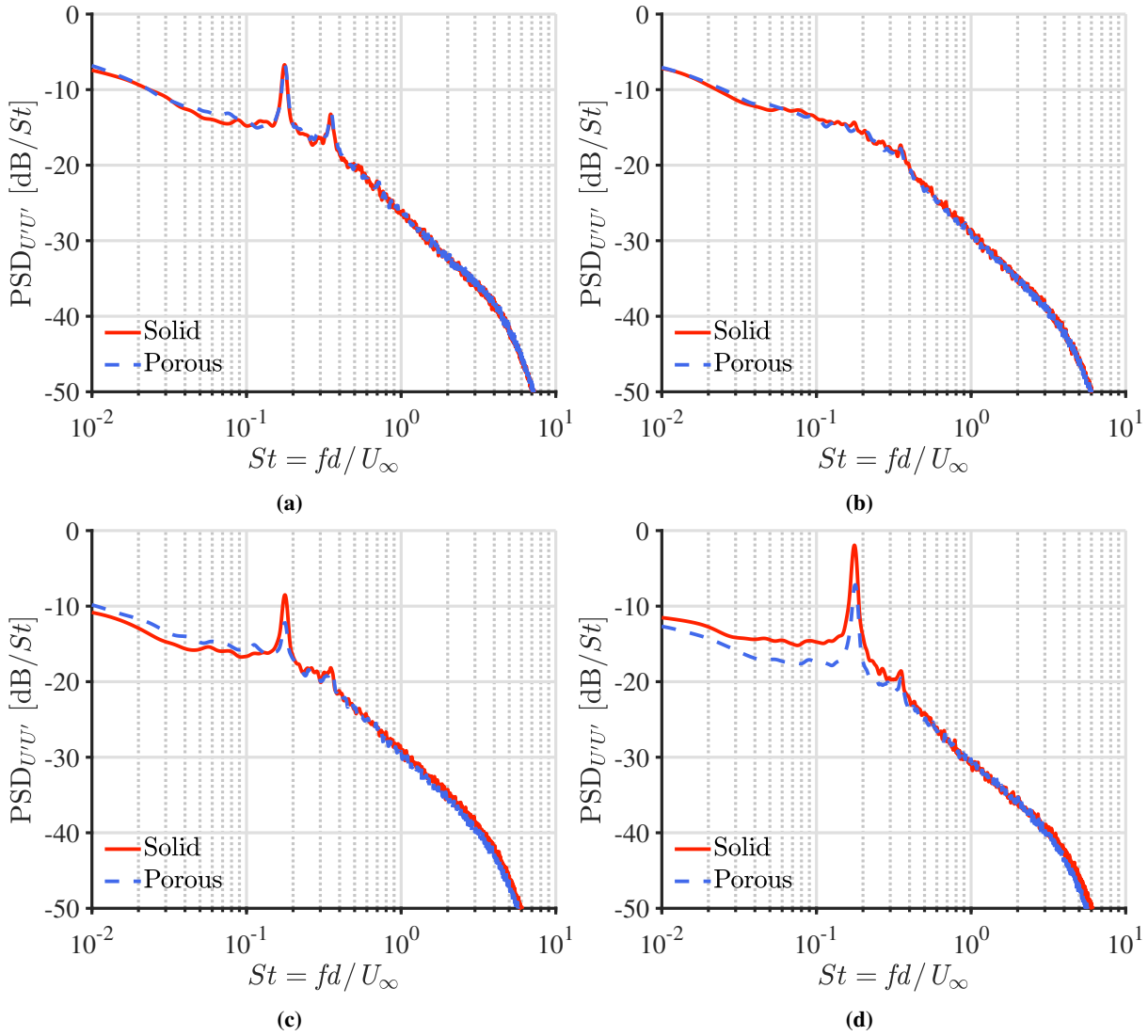


**Fig. 12 Velocity-fluctuation PSD for the solid (solid red line) and the porous case (dashed blue line) computed from the hot-wire measurements at (a) $\xi = x/r_{LE} = -6.7$, (b) $\xi = -1$, (c) $\xi = -0.5$, and (d) $\xi = -0.05$ with a reference of $1\ \mathrm{m^2\ s^{-1}}$.**

The PSDs of the velocity fluctuations from the experimental data extracted at four specific locations along the stagnation streamline have been computed. The results in Fig. 12 are presented in dB/$St$ with a reference of $1\ \mathrm{m^2\ s^{-1}}$. The Strouhal number is based on the cylindrical rod diameter and the free-stream velocity.

The measured vortex shedding frequency is found to be at $St = 0.176 \pm 0.001$. This value is slightly lower than what is commonly reported for Reynolds numbers in the high sub-critical regime [51–53]. The discrepancy is most likely caused by the significant blockage of the rod with respect to the wind tunnel width. At $\xi = -6.7$ (Fig. 12a), the velocity power spectra clearly present two peaks corresponding to the vortex shedding frequency and its first harmonic. At this position, no difference can be detected between the solid and the porous case, as already observed in Fig. 11b.

At $\xi = -1$ (Fig. 12b), the two considered cases still exhibit the same trend but now the vortex shedding frequency peak turns out to be fully dampened and is no longer visible in the spectra. It has been observed that this peak gradually decreases from the region downstream of the rod up to $\xi = -2$, where it disappears. Interestingly, at this location, the r.m.s. velocity fluctuations measured by the hot-wire start reducing, as shown in Fig. 11b.

Furthermore, in this intermediate region, the turbulence is not yet distorted and the size of the largest eddies of the turbulent flow in the streamwise direction can be estimated by evaluating the streamwise integral length scale $L_x$ from the autocorrelation function of the hot-wire time signal and from the local mean-flow velocity [54] considering Taylor's frozen turbulence assumption. The resulting $L_x \approx 4.2\, r_{LE}$ will be used in Section V to interpret the velocity-fluctuation trends by means of the RDT.

At $\xi = -0.8$, the peak at $St = 0.176 \pm 0.001$ reappears for both airfoils and increases in magnitude as the stagnation point is approached. This phenomenon is typical for stagnation-point flows [55] and might be caused by the effect of the flow deceleration that excites the instability associated with the vortex shedding and present in the incoming flow. Indeed, the vorticity of sufficiently large-scale eddies properly oriented to be stretched can undergo amplification as these structures are convected towards the stagnation region.

Moreover, the solid and porous spectra start diverging from $\xi = -0.5$, consistently with the $U'$ trends in Fig. 11b. For the measurement point closest to the airfoil surface at $\xi = -0.05$ (Fig. 12d), the part of the power spectrum that is affected by the porosity is that at low Strouhal numbers, which corresponds to large vortical structures, whereas the high-$St$ region is mostly unaltered. This was also verified by the POD results obtained by Tamaro et al. [56].



## V. Discussion of the results: rapid distortion theory

The results of the investigation described in Section IV can be interpreted considering the RDT. Indeed, previous experimental studies [11, 57] have demonstrated that, in a region sufficiently close to the stagnation point, the inflow distortion experienced by an airfoil is similar to that caused by a cylinder that has the same radius as the tangent circle at the airfoil leading edge. The porous RDT model developed by Zamponi et al. [29] will be employed in this case. For more information about the model, the interested reader is referred to the aforementioned paper.

According to Hunt [12], there are two ways in which a solid bluff body can affect the incident turbulent flow:

- through the distortion of the vorticity field due to the potential effect of the body, which alters the mean-velocity field around it and upstream of it and leads to a deflection of the streamlines;
- through the pressure exerted by the body, which blocks the turbulence fluctuations by forcing the component of the incident velocity that is normal to its surface to be zero.

The first effect can be considered negligible if the streamwise integral length scale of the turbulent flow is much higher than the characteristic dimension of the body. For the airfoil case, the aforementioned condition can be expressed by $L_x \gg r_{LE}$. On the contrary, the body always exerts pressure on the flow, regardless of the ratio between the streamwise integral length scale of the turbulence and the leading-edge radius. The present mechanism is evident for a flat plate, which is characterized by $L_x/r_{LE} \to \infty$. In this extreme case, the vorticity field is almost unaffected by the presence of the body and the only contribution to the alteration of the turbulent velocity fluctuations comes from the second effect.

As shown in Section IV, the turbulence approaching the airfoils at $\xi = -2$ is characterized by $L_x/r_{LE} > 4$. Therefore, it is reasonable to assume that the contribution of the first mechanism is almost negligible. Moreover, the presence of the permeable exoskeleton allows for an alteration of the velocity fluctuations and has a limited impact on the mean-velocity field in the stagnation region, preserving the potential effect of the body. This makes it possible to model the porous airfoil with the RDT by imposing the same deviation in mean flow produced by the solid configuration. In Figure 13, the one-dimensional spectra $\Phi_{U'U'}$ of the incident turbulent velocity computed at $\xi = -0.05$ for $L_x/r_{LE} = 4.2$ are compared with the measurements of Fig. 12d.

The RDT predictions feature the same trend and the same $\Delta\Phi_{U'U'}$ as the experimental results at low $St$, although the turbulence downstream of the rod does not meet the condition of homogeneity and isotropy assumed by the theory [29]. This suggests that the relative alterations in turbulence distortion due to porosity are independent of the nature of the upstream flow. However, deviations occur in correspondence with the frequency peak related to the vortex shedding in the wake of the upstream rod, which is not modeled in the present case. Furthermore, the analytical results exhibit an underprediction at high $St$ that can be attributed to the limitations in the spatial-wavenumber domain considered in the theory, as explained in [29].

The present agreement indicates that porosity mainly acts on the second turbulence-distortion mechanism pointed out by Hunt and affects the momentum transfer that occurs between the streamwise and upwash velocity fluctuations due to the non-penetration condition. Indeed, for the porous case, the possibility for part of the incident velocity to

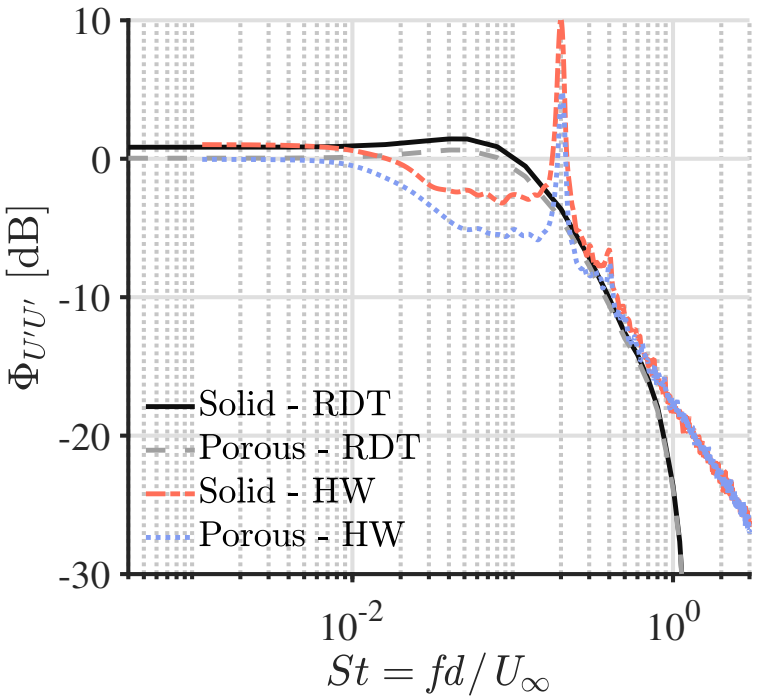


**Fig. 13 Comparison between the one-dimensional spectra of the incident turbulence measured by the hot-wire and the analytical predictions of the porous RDT model [29] for the solid and porous airfoil configurations. Data are taken at $\xi = -0.05$ for $U_\infty = 30\,\mathrm{m\,s^{-1}}$ and for a $0°$ angle of attack.**

penetrate the porous medium alters the velocity field around the airfoil and provides a non-zero velocity on the surface. This constitutes a reduced geometrical discontinuity with respect to a solid wall. Hence, the porous body exerts a lower pressure on the turbulence with respect to the solid one and this leads to a damping effect on the variation of the velocity fluctuations starting from $\xi = -0.5$, as discussed in Section IV. In view of the above, the distortion of the large vortical structures that interact with the porous airfoil leading edge is actually attenuated by the penetration of flow within the melamine foam. Physically, this dampened distortion leads to a decrease in the time variation of the inertia of the incoming turbulent gusts and therefore to less efficient conversion of their vortical energy into sound.

Finally, the fact that the turbulence is characterized by a large length scale compared to the characteristic dimension of the body implies that the dominant contribution to the incident-velocity power spectrum is given by the low-frequency range [12]. This explains why the influence of the porous treatment is visible mostly in this frequency range (Fig. 12d), in agreement with the analysis carried out by Tamaro et al. [56] and the trends of the integrated acoustic power spectra reported in Fig. 9. The aforementioned link confirms the key role played by the attenuation of the distortion of the turbulent eddies in the leading-edge noise reduction mechanism.

## VI. Conclusion

The present study aims at elucidating the physical mechanisms responsible for the turbulence-interaction noise reduction due to a porous treatment of a thick airfoil. A NACA-0024 profile has been integrated with melamine foam enclosed within a permeable exoskeleton in order to perform a comparison with a solid baseline. The two airfoils have been tested in a rod-airfoil configuration, at a Reynolds number based on the cylindrical rod diameter of $Re_d = 4.1 \times 10^4$.

The focus of the analysis has been put on the stagnation region near the leading edge with the purpose of examining the effect of the porosity on the distortion of the turbulent vortical structures in the interaction with the wing profiles. Specifically, from the acquisition of the mean wall-pressure distributions on their surface, it has been observed that the porous treatment leads to a slight reduction of the flow displacement by the airfoil due to the possibility for the incident velocity to penetrate the inner volume. This phenomenon influences the potential effect of the airfoil and levels out the pressure differences along the surface. However, the $C_p$ deviation between the two cases seems to be limited by the presence of the exoskeleton that preserves the integrity of the shape of the NACA-0024 profile.

Furthermore, the flow field along the stagnation streamline has been characterized by means of hot-wire anemometry. The experiments showed that the fluctuating velocity field is significantly affected by the porosity when the stagnation region is being approached. In particular, the significant increase of the r.m.s. of the upwash velocity fluctuations experienced by the solid airfoil in the immediate vicinity of the leading edge has not been observed in the porous case, resulting in an attenuation of the TKE in the stagnation region. Besides, the analysis of the turbulent velocity power spectra along the stagnation streamline and around the leading edge suggests that the melamine foam has an effect mainly at low frequencies on the large-scale structures. This is confirmed by the analytical predictions of the RDT. Therefore, the flow penetration through the pores of the melamine foam in the porous airfoil appears to soften the distortion of the largest turbulent eddies by the presence of the body. This is supported by the results of the acoustic beamforming measurements, which indicate that the most appreciable noise abatement is achieved in the one-third octave band containing the tonal component at the shedding frequency, showing a correlation with the attenuation of the turbulent velocity fluctuations.

In summary, the absence of a no-penetration condition on the surface of the porous airfoil reduces the time variation of the inertia of vortices, making the distortion *less rapid*, and eventually leads to less efficient conversion of vortical energy into sound. This hypothesis for explaining the role of porosity in the turbulence-interaction noise mitigation has been already formed in the past, but, to the authors' knowledge, no experimental evidence of it has ever been provided for a relatively thick airfoil.



## Acknowledgments

This project has received funding from the European Union's Horizon 2020 research and innovation program under the Marie Skłodowska-Curie grant agreement No. 722 401 in the framework of the ITN SmartAnswer. The authors would like also to thank Yves Aurégan from LAUM and Joachim Golliard from CTTM for the help and the support provided in the characterization of the porous medium parameters.

## References

[1] Zamponi, R., Satcunanathan, S., Moreau, S., Ragni, D., Meinke, M., Schröder, W., and Schram, C., "On the role of turbulence distortion on leading-edge noise reduction by means of porosity," *Journal of Sound and Vibration*, Vol. 485C, 2020, p. 115561. https://doi.org/10.1016/j.jsv.2020.115561.

[2] Zamponi, R., "Investigation of turbulence-surface interaction noise mechanisms and their reduction using porous materials," Ph.D. thesis, Delft University of Technology, Apr. 2021. https://doi.org/10.4233/uuid:d332c7e3-87be-4ed6-aa71-e629ef77e07a.

[3] Roger, M., Schram, C., and De Santana, L., "Reduction of Airfoil Turbulence-Impingement Noise by Means of Leading-Edge Serrations and/or Porous Material," *19th AIAA/CEAS Aeroacoustics Conference*, American Institute of Aeronautics and Astronautics, Berlin, Germany, 2013. https://doi.org/10.2514/6.2013-2108.

[4] Amiet, R. K., "Acoustic radiation from an airfoil in a turbulent stream," *Journal of Sound and Vibration*, Vol. 41, No. 4, 1975, pp. 407–420. https://doi.org/10.1016/S0022-460X(75)80105-2.

[5] Paterson, R., and Amiet, R., "Acoustic radiation and surface pressure characteristics of an airfoil due to incident turbulence," *3rd Aeroacoustics Conference*, American Institute of Aeronautics and Astronautics, Palo Alto,CA,U.S.A., 1976. https://doi.org/10.2514/6.1976-571.

[6] Olsen, W., and Wagner, J., "Effect of thickness on airfoil surface noise," *AIAA Journal*, Vol. 20, No. 3, 1982, pp. 437–439. https://doi.org/10.2514/3.7922.

[7] Oerlemans, S., and Migliore, P., "Aeroacoustic Wind Tunnel Tests of Wind Turbine Airfoils," *10th AIAA/CEAS Aeroacoustics Conference*, American Institute of Aeronautics and Astronautics, Manchester, UK, 2004. https://doi.org/10.2514/6.2004-3042.

[8] Moreau, S., Roger, M., and Jurdic, V., "Effect of Angle of Attack and Airfoil Shape on Turbulence-Interaction Noise," *11th AIAA/CEAS Aeroacoustics Conference*, American Institute of Aeronautics and Astronautics, Monterey, California, 2005. https://doi.org/10.2514/6.2005-2973.

[9] Devenport, W. J., Staubs, J. K., and Glegg, S. A., "Sound radiation from real airfoils in turbulence," *Journal of Sound and Vibration*, Vol. 329, No. 17, 2010, pp. 3470–3483. https://doi.org/10.1016/j.jsv.2010.02.022.

[10] Christophe, J., "Application of Hybrid Methods to High Frequency Aeroacoustics," Ph.D. thesis, Université Libre de Bruxelles, Nov. 2011.

[11] Santana, L. D., Christophe, J., Schram, C., and Desmet, W., "A Rapid Distortion Theory modified turbulence spectra for semi-analytical airfoil noise prediction," *Journal of Sound and Vibration*, Vol. 383, 2016, pp. 349–363. https://doi.org/10.1016/j.jsv.2016.07.026.

[12] Hunt, J. C. R., "A theory of turbulent flow round two-dimensional bluff bodies," *Journal of Fluid Mechanics*, Vol. 61, No. 4, 1973, pp. 625–706. https://doi.org/10.1017/S0022112073000893.

[13] Lee, S., "Reduction of blade-vortex interaction noise through porous leading edge," *AIAA Journal*, Vol. 32, No. 3, 1994, pp. 480–488. https://doi.org/10.2514/3.12011.

[14] Geyer, T., Sarradj, E., Giesler, J., and Hobracht, M., "Experimental assessment of the noise generated at the leading edge of porous airfoils using microphone array techniques," *17th AIAA/CEAS Aeroacoustics Conference (32nd AIAA Aeroacoustics Conference)*, American Institute of Aeronautics and Astronautics, Portland, Oregon, 2011. https://doi.org/10.2514/6.2011-2713.

[15] Geyer, T., Sarradj, E., and Giesler, J., "Application of a Beamforming Technique to the Measurement of Airfoil Leading Edge Noise," *Advances in Acoustics and Vibration*, Vol. 2012, 2012. https://doi.org/10.1155/2012/905461.

[16] Sarradj, E., and Geyer, T., "Symbolic regression modeling of noise generation at porous airfoils," *Journal of Sound and Vibration*, Vol. 333, No. 14, 2014, pp. 3189–3202. https://doi.org/10.1016/j.jsv.2014.02.037.

[17] Sarradj, E., and Geyer, T., "Noise Generation by Porous Airfoils," *13th AIAA/CEAS Aeroacoustics Conference (28th AIAA Aeroacoustics Conference)*, American Institute of Aeronautics and Astronautics, Rome, Italy, 2007. https://doi.org/10.2514/6.2007-3719.

[18] Teruna, C., Avallone, F., Casalino, D., and Ragni, D., "Numerical Investigation of Leading Edge Noise Reduction on a Rod-Airfoil Configuration Using Porous Materials and Serrations," *Journal of Sound and Vibration*, 2020, p. 115880. https://doi.org/10.1016/j.jsv.2020.115880.

[19] Roger, M., and Moreau, S., "Airfoil Turbulence-Impingement Noise Reduction by Porosity or Wavy Leading-Edge Cut: Experimental Investigations," *45th International Congress and Exposition on Noise Control Engineering*, INTER-NOISE, Hamburg, Germany, 2016, p. 10.

[20] Bampanis, G., and Roger, M., "On the Turbulence-Impingement Noise of a NACA-12 Airfoil with Porous Inclusions," *26th AIAA/CEAS Aeroacoustics Conference*, American Institute of Aeronautics and Astronautics, Virtual event, 2020. https://doi.org/10.2514/6.2020-2577.

[21] Geyer, T. F., Lucius, A., Schrödter, M., Schneider, M., and Sarradj, E., "Reduction of Turbulence Interaction Noise Through Airfoils With Perforated Leading Edges," *Acta Acustica united with Acustica*, Vol. 105, No. 1, 2019, pp. 109–122. https://doi.org/10.3813/AAA.919292.

[22] Avallone, F., Casalino, D., and Ragni, D., "Impingement of a propeller-slipstream on a leading edge with a flow-permeable insert: A computational aeroacoustic study," *International Journal of Aeroacoustics*, Vol. 17, No. 6-8, 2018, pp. 687–711. https://doi.org/10.1177/1475472X18788961.

[23] Sinnige, T., Corte, B. D., De Vries, R., Avallone, F., Merino-Martínez, R., Ragni, D., Eitelberg, G., and Veldhuis, L. L. M., "Alleviation of Propeller-Slipstream-Induced Unsteady Pylon Loading by a Flow-Permeable Leading Edge," *Journal of Aircraft*, Vol. 56, No. 3, 2019, pp. 1214–1230. https://doi.org/10.2514/1.C035250.

[24] Paruchuri, C., Joseph, P., Chong, T. P., Priddin, M., and Ayton, L. J., "On the noise reduction mechanisms of porous aerofoil leading edges," *Journal of Sound and Vibration*, Vol. 485, 2020, p. 115574. https://doi.org/10.1016/j.jsv.2020.115574.

[25] Kuczmarski, M., and Johnston, J., "Acoustic Absorption in Porous Materials," Technical Report NASA/TM-2011-216995, NASA Glenn Research Center, 2011.

[26] Zamponi, R., Ragni, D., Van de Wyer, N., and Schram, C., "Experimental Investigation of Airfoil Turbulence-Impingement Noise Reduction Using Porous Treatment," *25th AIAA/CEAS Aeroacoustics Conference*, American Institute of Aeronautics and Astronautics, Delft, The Netherlands, 2019. https://doi.org/10.2514/6.2019-2649.

[27] Satcunanathan, S., Meinke, M. H., and Schröder, W., "Prediction of Noise Mitigation by Porous Media based on a Direct-Hybrid CFD/CAA Method," *25th AIAA/CEAS Aeroacoustics Conference*, American Institute of Aeronautics and Astronautics, Delft, The Netherlands, 2019. https://doi.org/10.2514/6.2019-2696.

[28] Jacob, M. C., Boudet, J., Casalino, D., and Michard, M., "A rod-airfoil experiment as a benchmark for broadband noise modeling," *Theoretical and Computational Fluid Dynamics*, Vol. 19, No. 3, 2005, pp. 171–196. https://doi.org/10.1007/s00162-004-0108-6.

[29] Zamponi, R., Moreau, S., and Schram, C., "Rapid distortion theory of turbulent flow around a porous cylinder," *Journal of Fluid Mechanics*, Vol. 915, 2021, p. A27. https://doi.org/10.1017/jfm.2021.8.

[30] de Santana, L. D., "Semi-analytical methodologies for airfoil noise prediction," Ph.D. thesis, KU Leuven, Jun. 2015.

[31] Devenport, W. J., Simpson, R. L., Dewitz, M. B., and Agarwal, N. K., "Effects of a leading-edge fillet on the flow past an appendage-body junction," *AIAA Journal*, Vol. 30, No. 9, 1992, pp. 2177–2183. https://doi.org/10.2514/3.11201.

[32] Johnson, D. L., Koplik, J., and Dashen, R., "Theory of dynamic permeability and tortuosity in fluid-saturated porous media," *Journal of Fluid Mechanics*, Vol. 176, No. -1, 1987, p. 379. https://doi.org/10.1017/S0022112087000727.

[33] Champoux, Y., and Allard, J., "Dynamic tortuosity and bulk modulus in air-saturated porous media," *Journal of Applied Physics*, Vol. 70, No. 4, 1991, pp. 1975–1979. https://doi.org/10.1063/1.349482.

[34] Lafarge, D., Lemarinier, P., Allard, J. F., and Tarnow, V., "Dynamic compressibility of air in porous structures at audible frequencies," *The Journal of the Acoustical Society of America*, Vol. 102, No. 4, 1997, pp. 1995–2006. https://doi.org/10.1121/1.419690.

[35] Niskanen, M., Groby, J.-P., Duclos, A., Dazel, O., Le Roux, J. C., Poulain, N., Huttunen, T., and Lähivaara, T., "Deterministic and statistical characterization of rigid frame porous materials from impedance tube measurements," *The Journal of the Acoustical Society of America*, Vol. 142, No. 4, 2017, pp. 2407–2418. https://doi.org/10.1121/1.5008742.

[36] Satcunathan, S., Zamponi, R., Meinke, M., Van de Wyer, N., Schram, C., and Schröder, W., "Validation of a model for acoustic absorption in porous media," *48th International Congress and Exhibition on Noise Control Engineering*, INTER-NOISE, Madrid, Spain, 2019.

[37] Bruun, H. H., "Hot-Wire Anemometry: Principles and Signal Analysis," *Measurement Science and Technology*, Vol. 7, No. 10, 1996. https://doi.org/10.1088/0957-0233/7/10/024.

[38] Welch, P., "The use of fast Fourier transform for the estimation of power spectra: A method based on time averaging over short, modified periodograms," *IEEE Transactions on Audio and Electroacoustics*, Vol. 15, No. 2, 1967, pp. 70–73. https://doi.org/10.1109/TAU.1967.1161901.

[39] Dougherty, R. P., "Spiral-shaped Array for Broadband Imaging," Pat. US 5,838,284, 1998.

[40] Zamponi, R., de Wyer, N. V., and Schram, C., "An Improved Regularization of the Generalized Inverse Beamforming Applied to a Benchmark Database," *7th Berlin Beamforming Conference*, BeBeC, Berlin, Germany, 2018.

[41] Zamponi, R., Van de Wyer, N., and Schram, C., "Benchmark Assessment of an Improved Regularization Technique for Generalized Inverse Beamforming," *2018 AIAA/CEAS Aeroacoustics Conference*, American Institute of Aeronautics and Astronautics, Atlanta, Georgia, 2018. https://doi.org/10.2514/6.2018-4106.

[42] Merino-Martínez, R., Sijtsma, P., Carpio, A. R., Zamponi, R., Luesutthiviboon, S., Malgoezar, A. M., Snellen, M., Schram, C., and Simons, D. G., "Integration methods for distributed sound sources," *International Journal of Aeroacoustics*, Vol. 18, No. 4-5, 2019, pp. 444–469. https://doi.org/10.1177/1475472X19852945.

[43] Merino-Martínez, R., Luesutthiviboon, S., Zamponi, R., Rubio Carpio, A., Ragni, D., Sijtsma, P., Snellen, M., and Schram, C., "Assessment of the accuracy of microphone array methods for aeroacoustic measurements," *Journal of Sound and Vibration*, Vol. 470, 2020, p. 115176. https://doi.org/10.1016/j.jsv.2020.115176.

[44] Sijtsma, P., "Phased Array Beamforming Applied to Wind Tunnel And Fly-Over Tests," Tech. rep., National Aerospace Laboratory NLR, Oct. 2010.

[45] Bahr, C. J., and Horne, W. C., "Advanced Background Subtraction Applied to Aeroacoustic Wind Tunnel Testing," *21st AIAA/CEAS Aeroacoustics Conference*, American Institute of Aeronautics and Astronautics, Dallas, TX, 2015. https://doi.org/10.2514/6.2015-3272.

[46] Suzuki, T., "L1 generalized inverse beam-forming algorithm resolving coherent/incoherent, distributed and multipole sources," *Journal of Sound and Vibration*, Vol. 330, No. 24, 2011, pp. 5835–5851. https://doi.org/10.1016/j.jsv.2011.05.021.

[47] Zamponi, R., Chiariotti, P., Battista, G., Schram, C., and Castellini, P., "3D Generalized Inverse Beamforming in wind tunnel aeroacoustic testing: application to a Counter Rotating Open Rotor aircraft model," *Applied Acoustics*, Vol. 163, 2020, p. 107229. https://doi.org/10.1016/j.apacoust.2020.107229.

[48] Priddin, M. J., Paruchuri, C. C., Joseph, P., and Ayton, L. J., "A Semi-analytic and Experimental Study of Porous Leading Edges," *25th AIAA/CEAS Aeroacoustics Conference*, American Institute of Aeronautics and Astronautics, Delft, The Netherlands, 2019. https://doi.org/10.2514/6.2019-2552.

[49] Geyer, T., Sarradj, E., and Fritzsche, C., "Measurement of the noise generation at the trailing edge of porous airfoils," *Experiments in Fluids*, Vol. 48, No. 2, 2010, pp. 291–308. https://doi.org/10.1007/s00348-009-0739-x.

[50] Vagt, J.-D., "Hot-wire probes in low speed flow," *Progress in Aerospace Sciences*, Vol. 18, 1979, pp. 271–323. https://doi.org/10.1016/0376-0421(77)90010-0.

[51] Achenbach, E., "Vortex shedding from spheres," *Journal of Fluid Mechanics*, Vol. 62, No. 2, 1974, pp. 209–221. https://doi.org/10.1017/S0022112074000644.

[52] Giret, J.-C., Sengissen, A., Moreau, S., Sanjose, M., and Jouhaud, J.-C., "Noise Source Analysis of a Rod–Airfoil Configuration Using Unstructured Large-Eddy Simulation," *AIAA Journal*, Vol. 53, No. 4, 2015, pp. 1062–1077. https://doi.org/10.2514/1.J053371.

[53] Zhang, C., Sanjose, M., and Moreau, S., "Turbulent flow and noise sources on a circular cylinder in the critical regime," *Advances*, Vol. 9, 2019, pp. 085009 1–16. https://doi.org/10.1063/1.5121544.

[54] Swamy, N. V. C., Gowda, B. H. L., and Lakshminath, V. R., "Auto-correlation measurements and integral time scales in three-dimensional turbulent boundary layers," *Applied Scientific Research*, Vol. 35, No. 4, 1979, pp. 237–249. https://doi.org/10.1007/BF00418215.

[55] Sutera, S. P., Maeder, P. F., and Kestin, J., "On the sensitivity of heat transfer in the stagnation-point boundary layer to free-stream vorticity," *Journal of Fluid Mechanics*, Vol. 16, No. 4, 1963, pp. 497–520. https://doi.org/10.1017/S0022112063000963.

[56] Tamaro, S., Zamponi, R., Ragni, D., Teruna, C., and Schram, C., "Experimental investigation of turbulent coherent structures interacting with a porous airfoil," *Experiments in Fluids*, Vol. 62, 2021, p. 94. https://doi.org/10.1007/s00348-021-03170-2.

[57] Mish, P. F., and Devenport, W. J., "An experimental investigation of unsteady surface pressure on an airfoil in turbulence—Part 2: Sources and prediction of mean loading effects," *Journal of Sound and Vibration*, Vol. 296, No. 3, 2006, pp. 447–460. https://doi.org/10.1016/j.jsv.2005.08.009.